Chapter 1

Preferential Pathways: Drivers Of Temporal And Spatial Variability In Vapor Intrusion

1.1 Summary

Preferential pathways have recently been recognized for the significant role that they may play in enhancing vapor intrusion (VI). The nature and specific effect of a preferential pathway can vary greatly and is largely site specific; generalizing their impact can therefore be difficult. Two well-studied VI sites were revealed to be characterized by preferential pathways, providing an excellent opportunity to explore their influence. One of these sites was in Layton, Utah, which featured a preferential pathway that had a very significant impact on, among other things, but in particular, the temporal variability of indoor contaminant concentration. This preferential pathway was at a later date closed, and the comparison between the periods before and after the closing offers some unprecedented opportunities for understanding preferential pathways. A preferential pathway similar to that one will be implemented in our numerical model, and through analysis of data from the site, will offer insights how preferential pathways can enhance VI. The implications

of these insights have wider consequences for VI investigations in general, which is further explored in Chapter (TBD). Another well-studied site in Indianapolis, Indiana, was also affected by a preferential pathway, but its role and influence was very different from the Layton site, and in particular played a significant role in the spatial variability of subsurface contaminant concentrations, a topic which will explored using data from the site, as well as from the Layton site.

1.2 Introduction

Long term vapor intrusion (VI) studies in both residential and larger commercial structures have raised concerns regarding significant observed transient behavior in indoor air contaminant concentrations of anthropogenic origin[**u.s.˙environmental˙protection˙a folkes˙observed˙2009**, **holton˙temporal˙2013**, **johnston˙spatiotemporal˙2014**, **hosangadi˙high-frequency˙2017**, **mchugh˙recent˙2017**, **u.s.˙environmental˙protection˙ag** a phenomenon that has previously been observed at houses impacted by radon intrusion[**hubbard˙time-variation˙1996**]. Such variations make it difficult for those charged with protecting human health to formulate a response and conduct appropriate risk evaluation. Furthermore there is uncertainty within the VI community regarding how to best develop sampling strategies to address this problem[**u.s.˙environmental˙pr holton˙temporal˙2013**, **johnson˙integrated˙2016**, **mchugh˙recent˙2017**].

To address these concerns, two groups concerned with vapor intrusion researched purchased two different VI impacted houses and outfitted them with a wide variety of sensors and sampling instrumentation to study VI at these houses in great detail. Indoor contaminant concentration as well soil-gas and groundwater contaminant concentration at different depths and locations were recorded, while simultaneously recording metrics such as indoor and outdoor temperature, wind speed and direction, and building pressurization. These measurements were taken continuously over multiple years an unprecedented detailed dataset for exploring VI.

One of these houses was in Layton, Utah, near Hill AFB, and was purchased by a research group at Arizona State University (ASU), who conducted most of the

research at the site - this site will be referred to as the "ASU house" throughout this work[**holton˙temporal˙2013**]. The other was in duplex in Indianapolis, Indiana, purchased by the U.S. EPA and will be referred to as the "EPA duplex". There work was performed by multiple groups.

One thing both of these sites had in common was that after a few years of study, preferential pathways were discovered at the sites. A preferential pathway is typically thought of as some conduit that can transport large amounts of contaminant vapors into a building, in contrast with the slower vapor transport through soils.

At the ASU house, this took the form of a land drain underneath the house foundation, presumably installed during earlier house construction to drain excess water from the sub-slab region. This land drain was connected to the nearby sewer and its entrance as in a gravel layer under the house foundation, near a breach in the slab. The sewer it connected to was buried deep enough to be partially submerged in the TCE contaminated groundwater, which likely infiltrated into the sewer. The land drain when discovered was later excavated and fitted with a valve, allowing the researchers to control its influence - which was revealed to be very significant[**guo˙identification˙2015**]. The details of this is covered further below.

At the EPA duplex, the sewer acted as a preferential pathway, somewhat similar to the ASU house, but the nature of this preferential pathway was quite different from the one at the ASU house. A tracer gas test demonstrated that contaminant vapors were directly transported into the duplex[**mchugh˙evidence˙2017**]; similar to a site in Boston, Massachusetts, where PCE was transported into a bathroom through broken plumbing fixtures[**pennell˙sewer˙2013**]. It was also demonstrated that contaminated groundwater infiltrated into the sewer from a few blocks away from the duplex, where a dry-cleaners had previously been. This type of distributed contamination via a sewer network has likewise been recorded in Denmark[**nielsen˙remediation˙2017**] as a VI source - giving rise to a very different situation compared to radon intrusion or vapor intrusion from a groundwater source involving no preferential pathway.

It is also likely that the sewer pipe at the duplex leaked contaminant vapors somewhere near the vicinity of the house. This would give a situation that is similar to the ASU house land drain, but somewhat mitigated since the pipe leakiness was likely due to structural degradation, e.g. cracks in the mantle area; quite different from open channel flow from the ASU house land drain that brought contaminated air directly to the sub-slab area.

These studies shows some of the diverse ways that a preferential pathway can play a role in VI (Figure 1.1 shows a visual summary of these ways), and our illustrate often poor understanding in evaluating their significance. However, since the influence of the preferential pathway at the ASU house was able to be turned on and off (via the valve), we have an unprecedented opportunity to explore the effects of such a preferential pathway at a VI site.

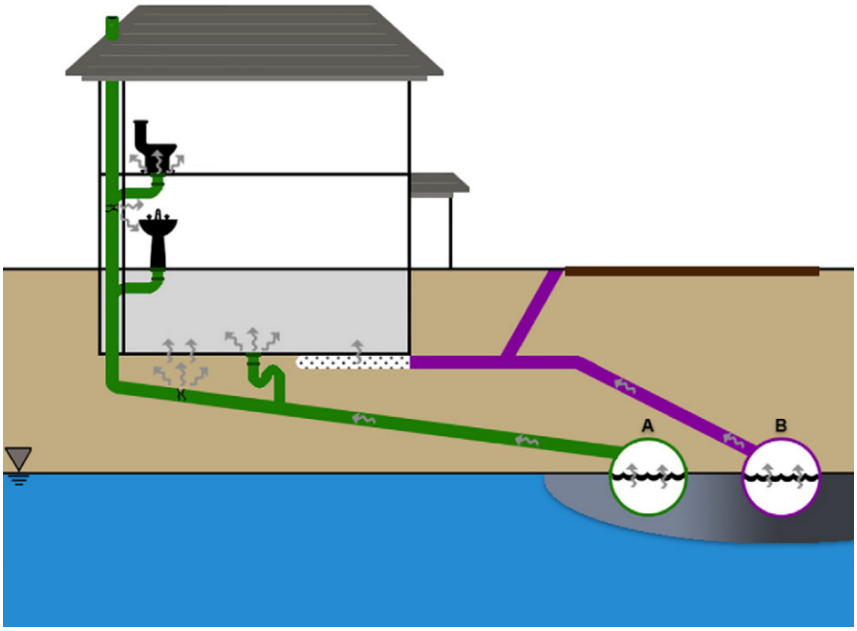

Figure 1.1: Visual summary of some of the different ways that contaminant can transport into a VI affected building via preferential pathways. Figure from **mchugˑevidenceˑ2017**[**mchughˑevidenceˑ2017**].

1.2.1 The ASU House

The VI study at the ASU house had two primary purposes:

1. Investigate VI with a particular focus on understanding the temporal and

spatial variability.

2. Test and evaluate the performance of the controlled pressure method (CPM).

This was to be achieved by monitoring various metrics relevant to VI, such as building pressurization, air exchange rate, indoor and outdoor temperature, and other metrological variables, while simultaneously monitoring the indoor air contaminant concentration. Additionally, soil-gas and groundwater contaminant concentration underneath and around the house were monitored; the specific sampling locations, as well as a photo of the house, can be seen in Figure 1.2a. The study of the ASU house is one of the most detailed studies of a VI site to date and fully describing the experimental setup and measured metrics is beyond the scope of this work but is detailed in **holton˙temporal˙2013**[**holton˙temporal˙2013**].

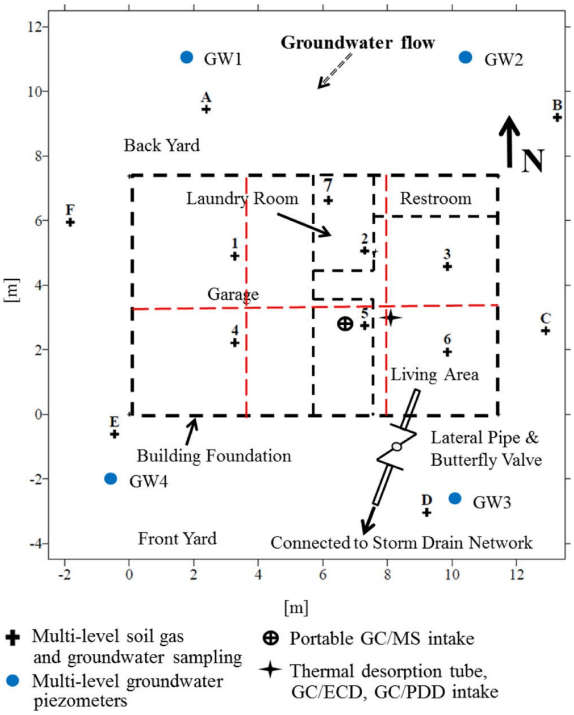

(a) Picture of the "ASU house" from **holton˙temporal˙2013**[**holton˙temporal˙2013**].

(b) Floor plan of the lower level of the "ASU house". Locations of all sampling ports and of the land drain preferential pathway marked. Figure from **guo˙identification˙2015**[**guo˙identification˙2015**].

CPM seeks to control the pressurization of the building, thereby controlling the contaminant entry rate. In this framework, overpressurizing a building will minimize or eliminate contaminant entry rate by VI into the building, thereby identifying

existence of indoor contaminant sources. By contrast, depressurizing a building will increase contaminant entry rate, giving a theoretical "worst-case" VI scenario. Here the researchers would used a 20 inch window box fan to control the pressurization of the building.

The site was monitored for roughly 1.5 years before the testing of the CPM system commenced. During this time, it was established that the indoor contaminant concentration fluctuated significantly at the site - roughly an order of magnitude on a weekly basis, while up to three or more orders of magnitude on a seasonal basis. Once the house was depressurized using the CPM system, indoor contaminant concentration increased to higher concentration levels previously recorded providing an initial verification of the CPM strategy[**holton˙long-term˙2015**].

However, during the CPM testing period, the researchers noticed that the house and nearby sewer seemingly communicated with each other. This was shown by the movement of a plastic tarp, which covered a nearby manhole, as the door of the house was opened and closed. This lead to the discovery of the land drain preferential pathway at the site; the location of it in relation to the house floorplan can be seen in Figure 1.2b The land drain was determined to exit into the gravel sublayer beneath the foundation, near a visible breach in the foundation slab, and was subsequently excavated and fitted with a butterfly valve [**guo˙identification˙2015**] to control its influence.

The land drain was closed towards the later part of the CPM study, which lead to a significant decrease in indoor contaminant concentration. This effect can be seen in Figure 1.3a, which shows the log-10 transformed indoor contaminant concentration for the entire study period. Here the pre- and post-CPM periods are marked by colors, and the closing of the land drain by the black vertical line. Notice how the temporal variability in indoor contaminant concentration decrease significantly after the closing of the land drain.

Figure 1.3b shows the same data, i.e. the log-10 transformed indoor contaminant concentration, but as a boxplot instead of a timeseries plot. Here the colored box

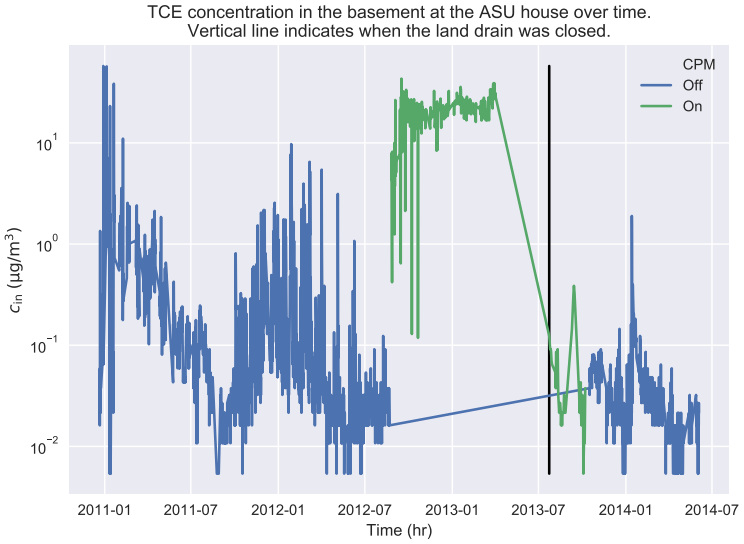

(a) The temporal variability of indoor air contaminant concentrations recorded at the ASU house. Measurements were taken in the basement. The periods during which the CPM system was on and off are marked.

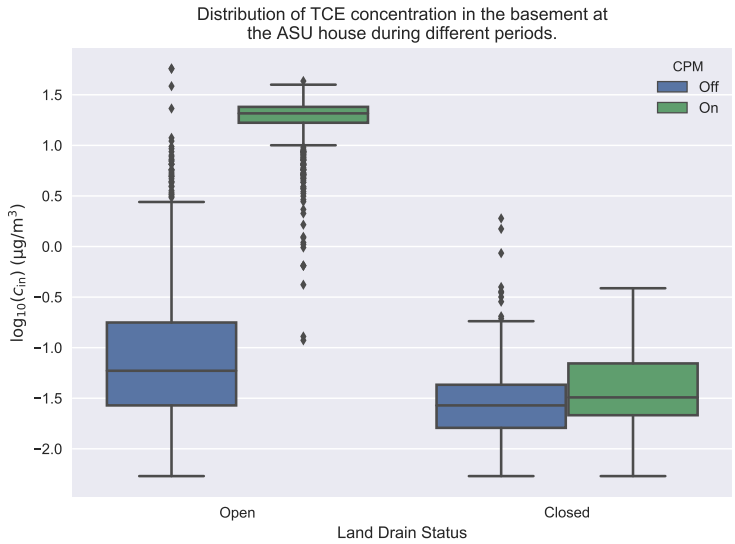

1

(b) Boxplot showing the log-10 transformed TCE concentrations at the ASU house. The CPM and natural periods, and the period before and after the land drain was closed are considered separately. The box signifies the interquartile range (IQR) of values, with the central line representing the median value, and the top and bottom of the box are the 25th and 75th percentiles. The whiskers extend to 1.5 times the IQR. Markers indicate outlier data points that fall outside the whiskers.

Figure 1.3

represents the interquartile range (IQR) of the distribution - the middle line is the 50th or median value, while the top and bottom of the represent the 75th and 25th percentile values. The whiskers are the extent of the dataset, while "outlier" points are given by the dots, here formally defined as data lying 1.5 times outside the IQR;

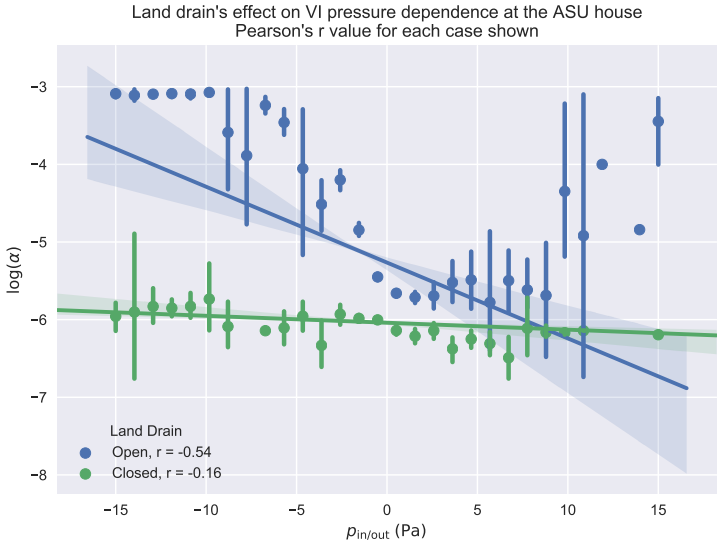

Figure 1.4: Regression plot showing the indoor/outdoor pressure difference dependence on indoor air concentration. Here the indoor air concentration is normalized to the groundwater source concentration, i.e. attenuation factor, and log-10 transformed. Data is placed in evenly spaced (but not sized) bins. The bars indicate the 95% confidence intervals.

these are "real" data points but simply plotted as outliers not to skew the IQR. This figure again reinforces the significant effect that the land drain preferential pathway had on the temporal indoor contaminant concentration variability at the ASU house.

In the VI field, it is widely held that the building depressurization relative to the ambient outdoor is a key driver of contaminant entry into VI impacted building. Since building pressurization fluctuations can occurs rapidly, this is a prime factor for investigating the transport dynamics of the preferential pathway. Figure 1.4 considers the relationship between the indoor air concentration and building pressurization, specifically indoor/outdoor pressure difference, for the periods when the preferential pathway was open and closed. This clearly shows the dramatic change in sensitivity of the indoor contaminant concentration to building pressurization after the closing of the preferential pathway, which is not only apparent from visual inspection but also from the change in the Pearson's r values for the considered periods. Pearson's r essentially tells us how good is a linear correlation between two datasets; a value of 1 indicates that there is a perfect positive linear relationship,

and -1 a perfectly negative linear relation. In our context, a negative value indicate that a decrease in building pressurization leads to an increase in indoor contaminant concentration, which makes sense as contaminant entry rates into the house would increase as it is further depressurized.

The question then becomes why this fundamental shift in the relationship between building pressurization and indoor contaminant concentration occurred, and how it relates to temporal variability in indoor contaminant concentration. Answering this is one of the primary objectives of this chapter, which will be done by developing a numerical model of a VI site that is *similar* to the ASU house, and in combination with comparison to the field data, will give insights how a preferential pathway can fundamentally alters contaminant transport at a VI site. We will also explore how such a preferential pathway can significantly contribute to the spatial variability in contaminant concentration, in particular in the near sub-surface region.

1.2.2 EPA Duplex

The EPA duplex was involved in, similarly to the ASU house, a highly detailed VI study; Figure 1.5a shows a photo of the site. Here the indoor contaminant concentrations of TCE, PCE, chloroform, and radon were measured in different floors of each side of the duplex, as well as in different locations and depths in the subsurface and groundwater - these sampling location ports, as well as a floorplan of the duplex can be seen in Figure 1.5b. These sampling ports also allowed pressure differences between different locations to be measured. Metrological data were collected throughout the study period, which lasted for around 2.5 years, and included indoor and outdoor temperatures, wind speed and direction, precipitation, and recorded snow coverage[**u.s.˙environmental˙protection˙agency˙assessment˙2015**]. The data from this site are publicly available online[**noauthor˙indianapolis˙nodate**].

This site was likewise characterized by significant temporal variability in indoor contaminant concentrations, which can be seen in Figure 1.6. This variability was not as significant as was recorded at the ASU house, but substantial nonetheless. Un-

(a) Photo of the EPA duplex. The right-hand side is the heated "422" side, while the left-hand side is the unheated "420" side.

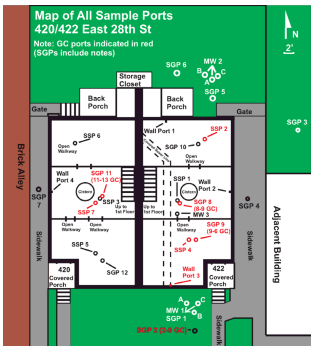

(b) Birdseye view of the EPA duplex, listing all the sampling location ports.

Figure 1.5

derstanding the observed variability was a major focus of this study, but additionally the researchers sought to evaluate the efficacy of a subslab depressurization (SSD) system. A SSD system depressurizes the subslab region, which diverts contaminant vapors from entering the structure into a pipe placed through the foundation slab, which then expells the vapors into the atmosphere[**u.s.˙environmental˙protection˙agency˙asse** There are many different possible configurations of these pipes, and their design is its own research topic, one which will not be addressed in this work. However, it is important to know when they were operated, and we will only consider data before the implementation of the SSD system. It should also be noted that only one side of the duplex was heated, and we will only consider data from this side.

Like the ASU house, it was later determined that a sewer preferential pathway existed at the site. This preferential pathway seemingly played a very different role than the one found at the ASU house, and different in primarily two ways:

1. Infiltration of contaminant vapors into the sewer did not occur near the duplex, but instead occurred a few blocks away - at the site of an old dry cleaner.

2. Communication between this preferential pathway and the indoor environment does not seem to have been as strong; the researchers believe that this may be due to the poor condition of the sewer pipe, which may have leaked somewhere along its path.

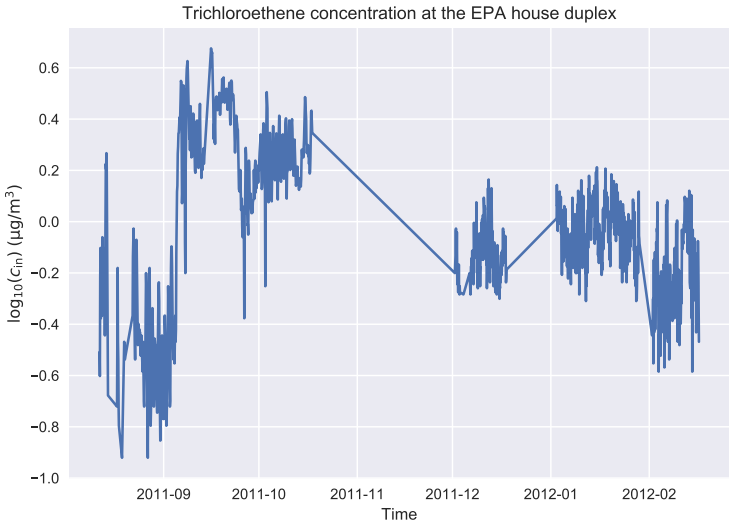

(a) Time series plot of the indoor TCE concentration in the heated side of the EPA duplex. Only the period before the SSD system was turned on considered.

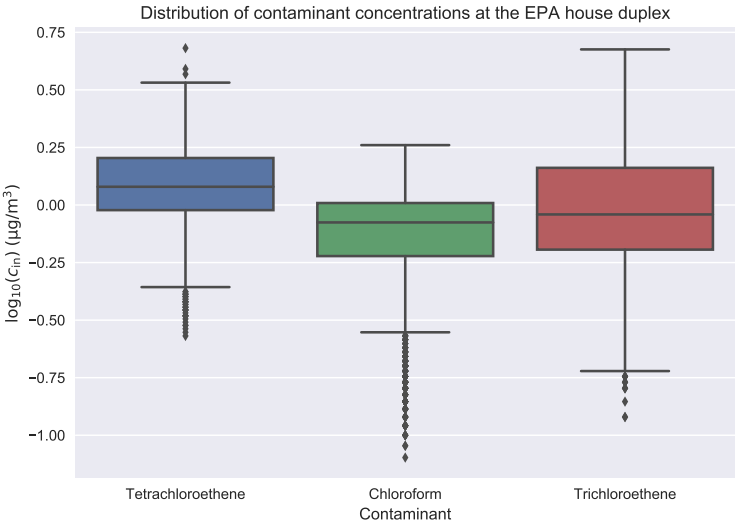

(b) Boxplot showing the distribution of log-10 transformed indoor concentration of three different contaminants in the heated side of the EPA duplex. The box is the interquartile range, with the line in the middle representing the median, and the top and bottom of the box representing the 75th and 25th percentiles respectively. The whiskers denote the extent of the data, with the points classified as "outliers", and are defined to be 1.5 times the IQR range.

Figure 1.6

The first of these points was demonstrated by **mchug˙evidence˙2017**[**mchug˙evidence˙2017**], which tracked contaminant vapors along the length of the sewer system. The second point, or rather the evidence that communication between the indoor environment and the preferential pathway may not have been so strong is indicated by

the lower temporal indoor contaminant concentration variability. It is also indicated by the weaker association between indoor contaminant concentration and the indoor/outdoor pressure difference, which can be seen in Figure 1.7; this weaker association is indicated by the smaller Pearson's r values compared to the ones at the ASU house before he closing of that preferential pathway.

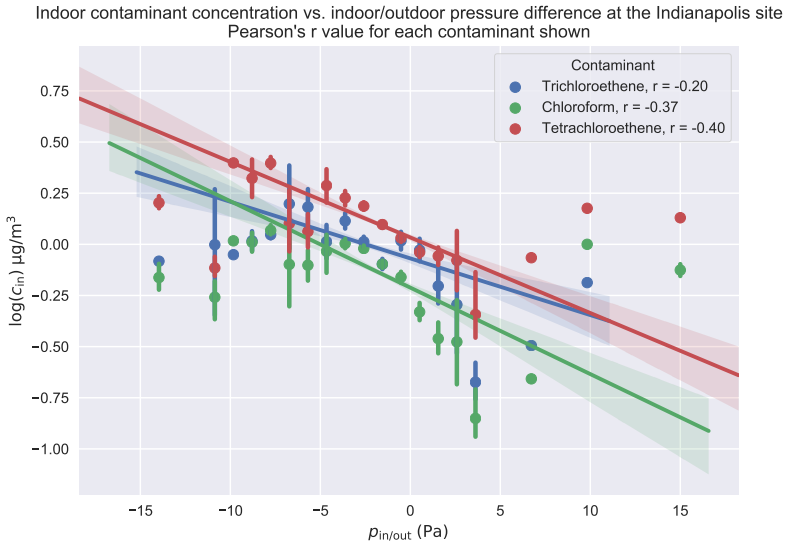

Figure 1.7: Relationship between indoor/outdoor pressure difference and indoor contaminant concentration of three contaminants - TCE, PCE, and chloroform at the EPA duplex.

Unfortunately, the EPA duplex preferential pathway is less well characterized, and its influence was never removed. This makes it difficult to assess how it contributed to overall VI at the site, or the observed temporal variability in indoor contaminant concentrations. However, it is possible to explore if the preferential pathway leaked somewhere near the site - which likewise will be a focus in this chapter.

Determining leakiness of the preferential pathway will be done by performing a kriging analysis of the measured soil-gas contaminant concentrations. Kriging is a type of interpolation technique which allows sparse data to be interpolated in multiple dimensions; ideal for interpolating soil-gas contaminant concentration in the soil surrounding the duplex. This way we can visually inspect the interpolated soil-gas contaminant concentration for "hot spots", which could indicate where such

a leak might be.

1.3 Modeling A Preferential Pathway

To investigate the role a land drain type preferential pathway may have on a VI site, we extend the VI model presented in Chapter **??**. By adding a gravel sub-base layer underneath the foundation slab and a preferential pathway to the earlier presented model, we develop a VI model scenario that is similar to the ASU house.

Here we assume the gravel sub-base layer is 30 cm thick and extends from the edges of the foundation slab. While the exact thickness of the gravel sub-base layer at the ASU house is not known, it was estimated to be roughly that thick. This is a typical thickness in US residential construction. The soil surrounding the house is assumed to be homogenous sandy clay. This is based on a description of the soil, and was chosen as the appropriate choice in modeling work by **guo˙vapor˙2015**[**guo˙vapor˙2015**], one of the researchers at the ASU house.

The gravel sub-base, unlike the rest of the soil, is relatively dry; it is covered by the foundation slab, so no rain infiltration will occur, and due to the coarseness of the gravel, no moisture will be drawn up by capillary forces. Nonetheless, some van Genuchten parameters for the gravel are necessary. Table **??** has the van Genuchten parameters used to model the soil and gravel.

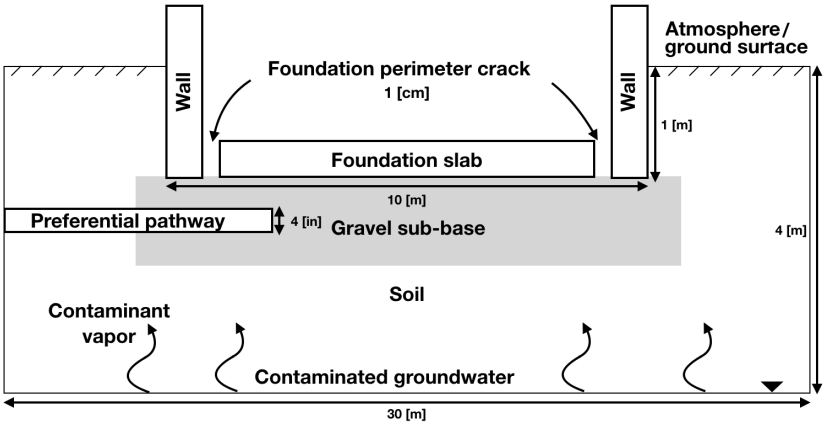

Figure 1.8: The modeled preferential pathway VI scenario.

Based on the description of the land drain preferential pathway at the ASU

site, we will model the preferential pathway as a 10 cm diameter pipe that exits at the interface between the soil and gravel sub-base layer. It terminates near the foundation crack - as was the case at the ASU house[**guo˙identification˙2015**]. Figure 1.8 shows the described scenario.

1.3.1 Geometry And Mesh

Explicitly modeling the entire preferential pathway in detail would requires a significant number of elements with little gain; contaminant vapor transport in the pathway itself is not of great interest. To save computational resources only the exit of the pipe is modeled as a 10 cm diameter circle representing the boundary between pipe and gravel.

With the addition of the preferential pathway pipe, only one plane of symmetry exists instead of two, and half of the domain model geometry has to be explicitly constructed instead of just a quarter of it as in Chapter **??**.

The meshing of the model follows the steps detailed in Chapter **??**, with the addition that a boundary layer mesh is generated on the preferential pathway exit plane. A similar initial mesh is generated as earlier, including subsequent adaptive mesh refinement. Figure 1.9 shows the resulting meshed geometry.

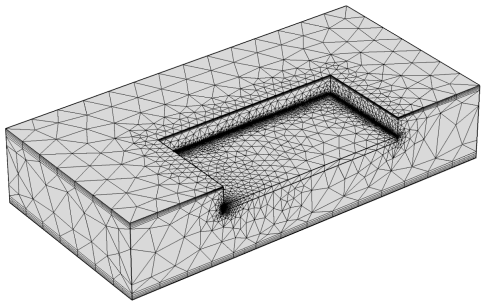

Figure 1.9: Meshed geometry of the preferential pathway model. Notice the gravel sub-base layer and the preferential pathway exit near the left hand foundation crack.

1.3.2 Physics And Boundary Conditions

In this model, we use the same governing equations introduced in Chapter **??**, but they are included here for completeness. However, to simulate the preferential pathway, we need to supply two new boundary conditions - one related to the airflow from the pipe, and another for the soil contaminant transport, which are discussed in their respective section below.

Indoor Environment

The indoor environment is still modeled using:

$$
\begin{aligned}
V_{\text{bldg}} \frac{\partial c_{\text{in}}}{\partial t} &= n_{\text{ck}} - V_{\text{bldg}} A_e c_{\text{in}} \\
n_{\text{ck}} &= \int_{A_{\text{ck}}} j_{\text{ck}} dA \\
j_{ck} &= \begin{cases} u_{ck} c_g - \frac{D_{\text{air}}}{L_{\text{slab}}} (c_{in} - c_g) & u_{ck} \geq 0 \\ u_{ck} c_{in} - \frac{D_{\text{air}}}{L_{\text{slab}}} (c_{in} - c_g) & u_{ck} < 0 \end{cases}
\end{aligned}
$$

c_{in} [$\text{mol}\,\text{m}^{-3}$] is the indoor contaminant concentration; n_{ck} [$\text{mol}\,\text{s}^{-1}$] is the contaminant entry rate into the building via the foundation crack; A_{ck} [m^2] is the foundation crack boundary area; $A_e = 0.5\,\text{h}^{-1}$ is the air exchange rate; $V_{\text{bldg}} = 300\,\text{m}^3$ is the volume of the house basement. $D_{\text{air}} = 7.2 \times 10^{-6}\,\text{m}^2\,\text{s}^{-1}$ is the diffusion coefficient of TCE in air; u_{ck} [$\text{m}\,\text{s}^{-1}$] is the airflow velocity through the foundation crack; $L_{\text{slab}} = 15\,\text{cm}$ is the thickness of the foundation slab; and c_g [$\text{mol}\,\text{m}^{-3}$] is the contaminant gas-phase concentration at the foundation crack boundary.

Soil Moisture

Soil moisture content is determined using van Genuchten's retention model. We use two "soil" types in this model - gravel and sandy clay; their parameters and

constants are shown in Table **??**.

$$\mathrm{Se} = \begin{cases} \frac{1}{(1+(\alpha|h|)^n)^m} & h < 0 \\ 1 & h \geq 0 \end{cases}$$

$$\theta_w = \begin{cases} \theta_r + \mathrm{Se}(\theta_t - \theta_r) & h < 0 \\ \theta_t & h \geq 0 \end{cases}$$

$$k_r = \begin{cases} \mathrm{Se}^l \left[1 - \left(1 - \mathrm{Se}^{\frac{1}{m}}\right)\right]^2 & h < 0 \\ 0 & h \geq 0 \end{cases}$$

$$\theta_g = \theta_t - \theta_w$$

h [m] is the elevation above the groundwater interface; Se is the saturation; α, m, $n = \frac{1}{1-m}$, $l = 0.5$ are the van Genuchten parameters; θ_w is the water filled porosity; θ_g is the gas filled pororsity; θ_t is the soil porosity; θ_r is the residual moisture content. and k_r is the relative permeability for water;

Soil Airflow

Airflow is still modeled using our modified Darcy's Law expression.

$$\frac{\partial}{\partial t}(\rho\theta_g) + \nabla \cdot \rho\Big(- \frac{(1-k_r)\kappa}{\mu}\nabla p\Big) = 0$$

$\vec{u}$ [$\mathrm{m\,s^{-1}}$] is the airflow velocity vector; κ [$\mathrm{m^2}$] is the permeability of the porous medium; μ [$\mathrm{Pa\,s}$] is the dynamic viscosity of the fluid; ∇p [$\mathrm{Pa\,m^{-1}}$] is the pressure gradient; θ_g is the gas-filled porosity of the soil; $\rho = 1.225\,\mathrm{kg\,m^{-3}}$ is the density of air; and $\mu = 18.5 \times 10^{-6}\,\mathrm{Pa\,s}$ is the dynamic viscosity of air. For steady-state cases, the first term is of course zero.

Boundary conditions Since the preferential pathway is assumed to be an open pipe, we assume it acts like a pressure gauge, and is at the reference ambient atmo-

spheric pressure.

Ground surface	$p = 0\,\text{Pa}$
Preferential pathway exit	$p = 0\,\text{Pa}$
Foundation crack	$p = p_{\text{in/out}}\,\text{Pa}$
Remaining boundaries	$-\vec{n} \cdot \rho\vec{u} = 0,$, i.e. no flow.

$p_{\text{in/out}}$ is not specified here as we will parametrically choose values for it.

Soil Contaminant Transport

The contaminant transport in the soil is governed by:

$$(\theta_w + \theta_g K_H)\frac{\partial c_w}{\partial t} = \nabla \cdot (D_{\text{eff}} \nabla c_w) - K_H \vec{u}_g \cdot \nabla c_w$$

c_w and c_g $[\text{mol}\,\text{m}^{-3}]$ are the contaminant concentrations in water and gas respectively; $K_H = 0.402$ is the dimensionless Henry's Law constant for TCE at 20 °C; $\vec{u}_g$ $[\text{m}\,\text{s}^{-1}]$ is the Darcy's velocity field; and D_{eff} $[\text{m}^2\,\text{s}^{-1}]$ is the effective diffusivity of the contaminant according to Millington-Quirks model:

$$D_{\text{eff}} = \left(D_w \frac{\theta_w^{\frac{10}{3}}}{\theta_t^2} + D_g \frac{\theta_g^{\frac{10}{3}}}{\theta_t^2} K_H\right)$$

$D_w = 1.02 \times 10^{-9}\,\text{m}^2\,\text{s}^{-1}$ and $D_g = 6.87 \times 10^{-6}\,\text{m}^2\,\text{s}^{-1}$ are the diffusion coefficient of TCE in water and air respectively. Again, $\frac{\partial c_w}{\partial t} = 0$ for steady-state cases.

Boundary conditions The air in the pipe is assumed to be contaminated with TCE at a vapor concentration c_g in equilibrium with the groundwater source contaminant concentration. This assumption is based on contaminant samples taken from a manhole near the ASU house[**guo˙vapor˙2015**] which demonstrated that contaminant vapor concentrations in the nearby sewer were of similar magnitude as

the contaminated groundwater source.

Atmosphere	$c_w = 0\,\mathrm{mol\,m^{-3}}$
Groundwater	$c_w = c_{gw}\ \mathrm{mol\,m^{-3}}$
Preferential pathway	$c_g = c_{gw}K_H\ \mathrm{mol\,m^{-3}}$
Foundation crack	$-\vec{n}\cdot\vec{N} = \dfrac{-j_{ck}}{K_H}\ \mathrm{mol\,m^{-2}\,s^{-1}}$
All other	$-\vec{n}\cdot\vec{N} = 0\,\mathrm{mol\,m^{-2}\,s^{-1}}$, i.e. no contaminant flux.

Note that we are neglecting any sorption in the soil, i.e. the sorption partitioning coefficient $K_p = 0\,\mathrm{m^3\,kg^{-1}}$, and this term does not enter in a steady-state analysis in any case. We will likewise normalize all concentrations to the source concentration c_{gw}, and any arbitrary value can be assigned.

1.4 Temporal Variability And Preferential Pathways

In the calculation results shown in Figure 1.10, a preferential pathway is assumed to provide air containing contaminant vapor at a concentration equivalent to the vapor in equilibrium with the underlying groundwater source. This shows the true importance of the preferential pathway - it brings contaminated vapors directly to the sub-slab without attenuation in concentration associated with diffusion through soil. Here, the indoor air exchange rate A_e was assumed to be a constant 0.5 per hour, and $p_{\mathrm{in/out}}$ was varied from -5 to 5 Pa. Values of predicted indoor air contaminant concentrations, c_{in} were obtained from steady state calculations. The predicted c_{in} values were then normalized by the assumed vapor concentration in equilibrium with groundwater c_{gw}, giving the attenuation from groundwater α_{gw}. The predicted values of α_{gw} as a function of $p_{\mathrm{in/out}}$ are given by the solid line Figure 1.10. These predicted values are compared to actual measured α_{gw} values from the ASU House for the period during which the preferential pathway was open given by

the blue points.

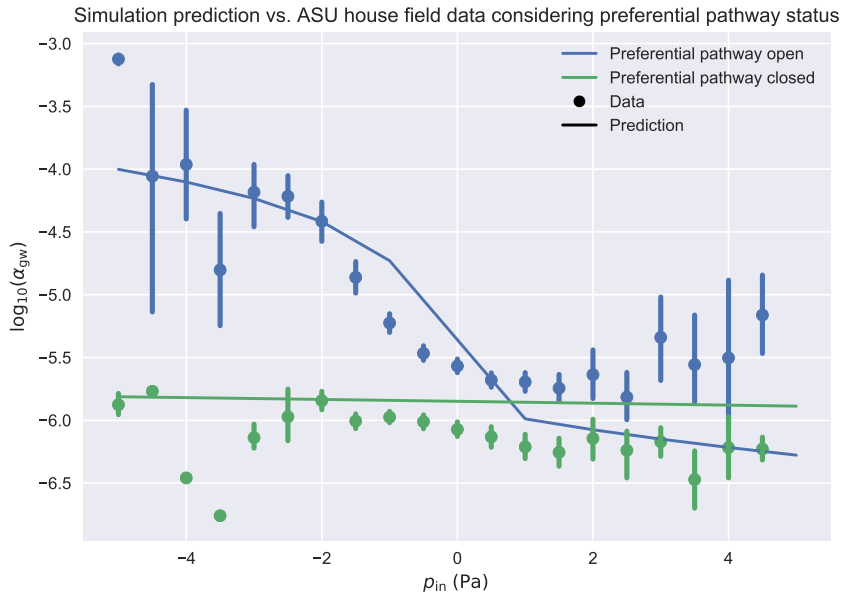

Figure 1.10: Model predicted indoor air concentration (as groundwater attenuation) compared to values recorded at the ASU house. The modeling results are given the solid lines and data by the dots. Blue here represents data before the closing of the preferential pathway and modeling result from the corresponding model, i.e. the model features a preferential pathway and a gravel sub-base. The green color signifies data from the period after the closing of the preferential pathway with the corresponding model, i.e. the preferential pathway is removed but the gravel sub-base remains. Here the data is placed in 20 equally *spaced bin*, i.e. not equally *sized*. The dot is the mean value and the error bars represent the 95% confidence intervals.

While the intent was not to exactly model all details of the ASU house, the model captures key details such as house footprint size, crack entry size, existence of a gravel sub-base, and a "land drain". The model successfully predicts the observed trends in α_{gw} as $p_{in/out}$ decreases (increased depressurization) but somewhat underpredicts α_{gw} as the house is overpressurized. Most significantly, the model captures that even for a small increase in depressurization (0 to -5 Pa) a very large increase in α_{gw} (two order of magnitude) can occur.

The model is also able to capture the weak trend in α_{gw} with $p_{in/out}$ when a preferential pathway is absent, but when there still exists a permeable subslab region. These results are given by the green line in Figure 1.10. These results are again in agreement with what was observed at the ASU House when the preferential

pathway was closed, i.e. that there was a much more modest variation in indoor air concentration, irrespective of pressure, when the preferential pathway was cut off.

The model corroborates the significant contribution that such a preferential pathway may have at a VI site. The preferential pathway acts not only as a source of contaminant vapor, but also as a source of air to the subslab. Because of the large resistance to soil gas flow in the surrounding soil, having a local source of air to support the increase of advective flow into the structure from the subslab region makes a large difference. (This will be examined below). While there obviously is still some variability unaccounted for, as indicated by the error bars on the actual field data in Figure 1.10, we can say with some confidence that the model is able to capture the general influence of a preferential pathway. This invites us exploring some of the factors that help explore more of the variability. Using our model, we rerun the scenarios, but this time consider two more cases:

1. We remove the gravel sub-base layer but keep the preferential pathway.

2. We keep the gravel sub-base layer, but remove contaminant vapor from the preferential pathway, i.e. it supplies only "clean" air.

The results of running these cases can be seen in Figure 1.11.

Here the original modeling results and associated data from the period before the closing of the preferential pathway are again given by blue points and curve. The case corresponding to the removal of contaminant vapors from the preferential pathway is shown by the green line, while the removal of the gravel sub-base care is shown by red.

The removal of contaminant vapors from the preferential pathway largely eliminates the significant dependence of α_{gw} on p_{in} as shown earlier by blue in Figure 1.10 (see the green curve). However, the increase in indoor air concentration with decreased indoor pressure is smaller than when the preferential pathway was present. This shows that a preferential pathway similar to the one found at the ASU house does two things.

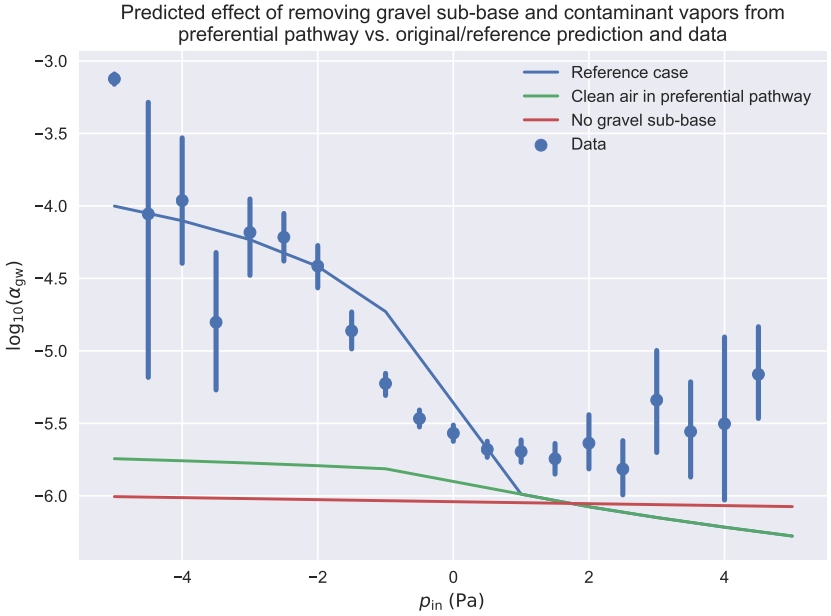

Figure 1.11: How different cases affect the predicted impact of the preferential pathway.

First, it provides a preferential source of air, and the depressurized building is able to much easier draw air from the preferential pathway than the surrounding soil; the soil offers a huge resistance to airflow and thus advective transport critical to contaminant entry. Second, the increase in "advective potential" alone is inadequate to cause the large effect as observed at the ASU house, and a preferential source of contaminant vapors is also required - two conditions that were fulfilled at the ASU house.

The removal of the gravel sub-base likewise also has a significant effect on the modeling results. Without it the full potential of a preferential pathway is unrealized (see the red curve). This can again be understood because of the significant resistance to contaminant transport that soils present. This adds a third condition for a preferential pathway to exert a significant influence - a medium for effective communication between the preferential pathway and indoor environment is necessary.

The importance of advective transport can be shown by analyzing the Péclet number for transport through the foundation crack. The Péclet number is a dimen-

sionless number defined as the ratio of advective to diffusive transport rate across some characteristic length, i.e. it tell us if transport is advective or diffusion dominated. For transport of contaminants through the foundation crack we define this as

$$\mathrm{Pe} = \frac{\text{advection}}{\text{diffusion}} = \frac{u_{\mathrm{ck}} L_{\mathrm{slab}}}{D_{\mathrm{g}}} \tag{1.1}$$

here u_{ck} $[\mathrm{m\,s^{-1}}]$ is the airflow velocity across (through) the crack $L_{\mathrm{slab}} = 15\,\mathrm{cm}$ is the thickness of the foundation slab, i.e. the characteristic length for transport; and $D_g = 6.87 \times 10^{-6}\,\mathrm{m^2\,s^{-1}}$ is the diffusivity of TCE in air.

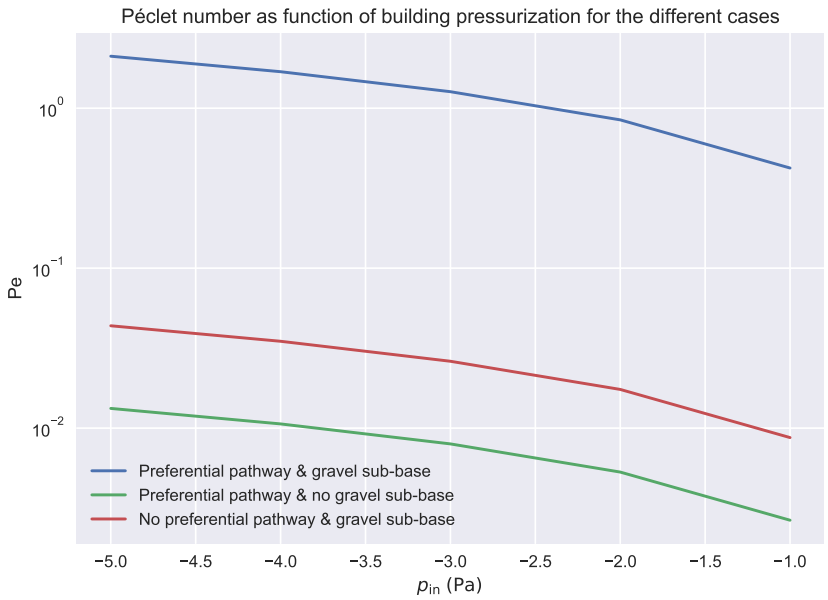

Figure 1.12: Péclet number for transport through the foundation crack of our modeled house as a fucntion of building pressurization. Here we consider three cases where the preferential pathway and gravel sub-base are present/absent, which shows the dramatic effect these site features can have on contaminant transport at a VI site.

The values of Pe characterize transport as:

$\mathrm{Pe} \gg 1$	Advection dominated
$\mathrm{Pe} \ll 1$	Diffusion dominated
$\mathrm{Pe} = 1$	Advection and diffusion equal

Figure 1.12 shows the Péclet number for three of the modeled cases:

1. Preferential pathway and gravel sub-base layer present
2. Preferential pathway present but gravel sub-base layer absent
3. Preferential pathway absent but gravel sub-base layer present

Note that the cases when $p_{\text{in}} > 0\,\text{Pa}$ are not shown. By our definition $u_{\text{ck}} > 0$ indicates airflow into the house, giving $\text{Pe} > 0$. This figure shows that it is only when there is a combination of a preferential pathway and a gravel sub-base layer that advective transport is able to dominate; diffusive transport dominates for the other cases which explains the weak correlation between α_{gw} and p_{in} in Figure 1.11 when the preferential pathway was removed. The rate of diffusion of TCE in air does not depend upon p_{in}. Likewise it explains the dramatic increase of α_{gw} as p_{in} decreases when the gravel sub-base and preferential pathway were present, as advective transport only starts to dominate after $p_{\text{in}} < -2.5\,\text{Pa}$.

To summarize, for a preferential pathway to have a significant influence at a VI site, the following conditions need to be fulfilled:

1. A preferential source of air in required to enhance the advective transport potential at the site.
2. Contaminant vapors must likewise be preferentially supplied.
3. There needs to exist a medium to facilitate effective communication between the preferential pathway and the indoor environment.

While this may seem like some specific conditions to be fulfilled for a preferential pathway to be so impactful, it can easily be generalized to other scenarios. For instance, one could easily imagine a situation where a house has a gravel backfill surrounding it, with some other subsurface source - like a leaky sewer pipe (that does not exit anywhere the building). Under such a circumstance, one could conceivably observe a similar effect in the indoor contaminant concentration caused by a very different scenario.

1.4.1 Role Of Air Exchange Rate

Simulations so far has assumed that the indoor air exchange rate is at a constant $0.5\,\mathrm{h}^{-1}$ irrespective of the house pressurization. This is not quite realistic, as air exchange rates are constantly fluctuating, and this will have an impact on indoor contaminant concentrations. To account for this, we rerun our model simulations, but this time assuming different air exchange rate values, and determine if this can capture some more of the observed variability.

Ideally, we would wish to be able to determine air exchange rate based on site conditions, and in particular building pressurization. Determining air exchange rate exactly is difficult, as it is influenced by building pressurization, indoor/outdoor temperature differences, wind, operation of HVAC systems, etc. This is a topic that will be expanded on in Chapter **??**.

Designed air exchange rates are often legally regulated as part of local building ordinances, and depending on the type of building, its values and bounds are usually more or less known. Here, we will rerun the model and assume a wide range of constant air exchange rate values. At the ASU house, air exchange rates were measured using a tracer-gas study, and the the 10th, 50th, and 90th percentile air exchange rate values are shown in Table 1.1. Also shown are the corresponding values from the EPA duplex, and those from an independent EPA study that measured air exchange rates nationwide. Based on this we rerun the model using air exchange values of 0.1, 0.5, and $0.9\,\mathrm{h}^{-1}$.

	Percenti	
	10th	50th
EPA study[**u.s.˙epa˙exposure˙2011**, **m.˙d.˙koontz˙estimation˙1995**]	0.16-0.2	0.35-0.49
ASU house[**holton˙temporal˙2013**, **guo˙identification˙2015**]	0.21	0.43
EPA duplex[**u.s.˙environmental˙protection˙agency˙assessment˙2015**]	0.34	0.74

Table 1.1: Air exchange rate values [h^{-1}]

Figure 1.13 shows the result of incorporating a wider range of air exchange rates when predicting α_{gw}. Here the central lines are the result corresponding to $A_e = 0.5\,\mathrm{h}^{-1}$, while the upper and lower bounds of each shaded area correspond to

$A_e = 0.1$ and $0.9\,\mathrm{h}^{-1}$ respectively. The shaded area cover much of the confidence interval of α_{gw} as a function of p_{in} This indicates that much of the uncertainty of numerically determining α_{gw} could be accounted for by considering the range of air exchange values at a site.

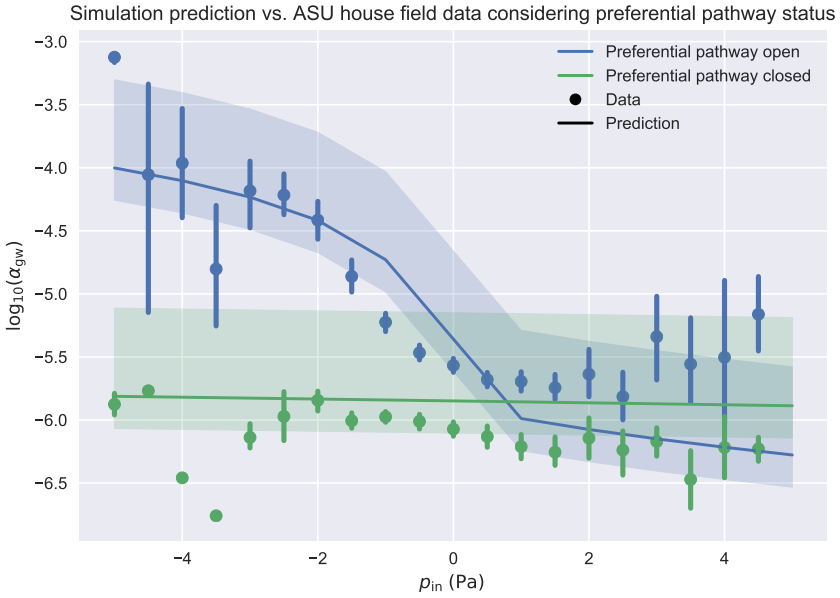

Figure 1.13: Modeling result from Figure 1.10 but with added shaded area to demonstrate the effect of assuming different air exchange values. The central lines are the result corresponding to $A_e = 0.5\,\mathrm{h}^{-1}$, while the upper and lower bounds of each shaded area correspond to $A_e = 0.1$ and $0.9\,\mathrm{h}^{-1}$ respectively.

The fact that indoor air pressure and air exchange rate can both vary is applied to a transient simulation, where we model a "typical" day at the ASU house by using the median diurnal variation of p_{in} and A_e as model inputs. We consider our model with and without the preferential pathway present. Specifically, we use the median diurnal values of p_{in} and A_e at one hour intervals over a 24-hour period and interpolate using cubic splines between these for continuity. This is compared to a case where we only use the median diurnal values of p_{in} but keep $A = 0.5\,\mathrm{h}^{-1}$ constant. Now the transient terms neglected at steady-state will be included.

Figure 1.14 shows how α_{gw} varies throughout this hypothetical "typical" day. Here we see that when the preferential pathway is present, variability of α_{gw} is mostly driven by fluctuations in contaminant entry rate; the variable and constant

air exchange rate cases do not differ much from each other. When the preferential pathway is absent, then there is no variability of α_{gw} unless the air exchange rate is fluctuating.

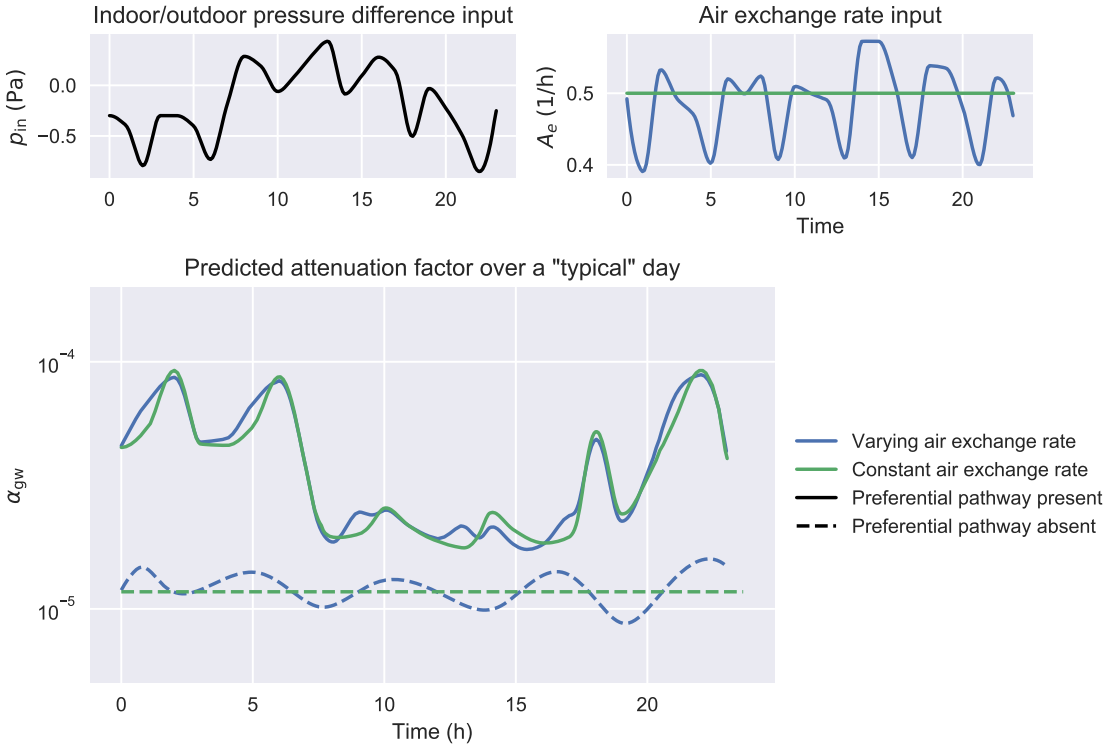

Figure 1.14: Modeled indoor contaminant concentration (as attenuation from groundwater) over a "typical" day. Here the hourly median indoor/outdoor pressure difference and air exchange rates recorded at the ASU house, as well as a comparison case where a constant air exchange rate of $0.5\,\mathrm{h}^{-1}$ is assumed, are used as model input parameters. For these we consider two models cases; one where a preferential pathway is present, and another in which it is absent respectively.

To quantify the predicted variability of α_{gw} we define ratio between the minimum and maximum α_{gw} as

$$\Delta_{max} = \frac{\alpha_{gw,max}}{\alpha_{gw,min}} \tag{1.2}$$

Applying this to the cases where air exchange rate is varied, and the preferential pathway present/absent we find that these ratios are $\Delta_{max} = 5.09$ and $\Delta_{max} = 1.68$ respectively. I.e. α_{gw} may be expected to vary around half an order of magnitude at a site characterized by a preferential pathway under our considered conditions, whereas one where there is no preferential pathway may vary by a factor of 1.68.

These "maximum daily variability" Δ_{max} values can be compared to those at

the ASU house. Indoor contaminant concentration samples at the ASU house were collected roughly every four hours across the study period. By excluding the CPM period, and then resampling these data on a daily basis, we can find $\Delta_{\max}$ for each day. These data are further separated to consider the period before and after the land drain preferential pathway was closed. The period before the preferential pathway was closed then includes 441 days or data points, giving a median value $\Delta_{\max} = 2.33$. For the period after the preferential pathway was closed, we get 181 days of data, giving a median value of $\Delta_{\max} = 1.60$. Thus, we can see that we somewhat overpredicted the expected variability for the period when the preferential pathway was open, but were quite close when it was closed.

This indicates that for sites that are characterized by diffusive transport, much of the observed variability of indoor contaminant concentrations are driven by fluctuations in air exchange rate. For sites dominated by advective transport, fluctuations in building pressurization, and consequently contaminant entry, are more important drivers for temporal variability of α_{gw}.

1.5 Soil-Gas Spatial Variability And Preferential Pathways

Preferential pathways can have a significant impact on spatial variability of contaminant vapors at a site. This can manifest inside a house itself, as large concentration differences between rooms, as was the case due to a leaky bathroom plumbing fixture in the work by **pennell˙sewer˙2013**[**pennell˙sewer˙2013**]; contaminant concentration was significantly higher in the upstairs bathroom than the basement, where higher concentrations are usually expected. Spatial variability in contaminant concentration can also manifest in the subsurface, which can be caused by a contaminant source[**chow˙concentration˙2007**], the building itself[**holton˙creation˙2018**], or as we will explore here - a subsurface preferential pathway.

1.5.1 ASU House

guo˙identification˙2015[**guo˙identification˙2015**] explored the role that the ASU house land drain preferential pathway had on the spatial variability of contaminant vapors in the subsurface, and in particular in the gravel sub-base. They used Kriging interpolation to visualize the distribution of subsurface contaminant vapors using their collected subsurface contaminant vapor samples. One snapshot of this work can be seen in Figure 1.15 where it clearly visible how the preferential pathway dramatically increased the contaminant vapor concentration in one half of the gravel sub-base layer - the half where the land drain preferential pathway exit was located.

While this demonstrates the influence of a preferential pathway on subsurface spatial variability, it can be quantitively explored just how significant it can be. To do this, we consider the attenuation from the sub-slab region to the indoor environment

$$\alpha_{\text{subslab}} = \frac{c_{\text{in}}}{c_{\text{subslab},5}} \tag{1.3}$$

using sub-slab vapor contaminant concentration data from location 5 of the ASU house (see Figure **??**). This was the sample location closest to exit of the land drain preferential pathway. These data are visualized in a boxplot in Figure 1.16 where we consider the effects of CPM and the land drain preferential pathway on α_{subslab}.

Here we observe that when the preferential pathway was open and the CPM system active, α_{subslab} usually exceeded unity by at least an order of magnitude, a situation that seemingly violates the expected concentration gradient from outside to indoors; we can likewise see that this is an observed occurrence when the preferential pathway was open but the CPM system inactive. Normally, one would not expect α_{subslab} to be even of the order of unity. Examining the α_{subslab} data from the period after the preferential pathway was closed, as well as α_{subslab} data collected by the EPA in their VI database, α_{subslab} would be expected to range from 1×10^{-3} to 1×10^{-1} with 3×10^{-2} a commonly encountered value[**u.s.˙environmental˙protection˙agency˙**
In other words, the process of transport from subslab to indoor involves a substantial concentration gradient. When $\alpha_{\text{subslab}} \geq 1$ this can be an indicator that even though

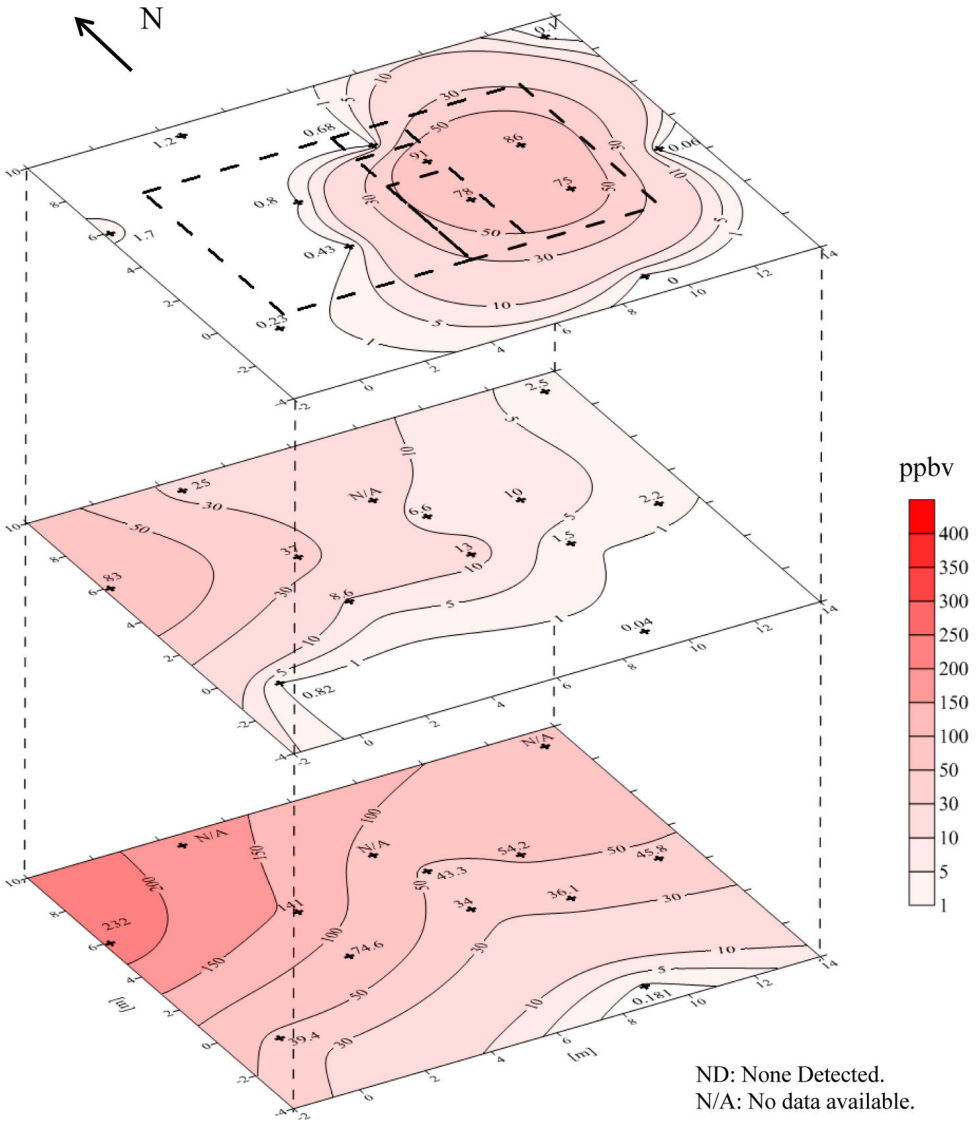

Figure 1.15: Distribution of TCE contaminant vapors in the subsurface underneath the ASU house. The top layer is right beneath the foundation, with the two subsequent at 0.9 m and 1.8 m below the foundation slab. Snapshot from the period when the CPM system was active. Figure from **guo˙identification˙2015**[**guo˙identification˙2015**].

location 5 is only 2 m away from the land drain preferential pathway exit, samples taken here may fail to capture the highest sub-slab contaminant concentrations; the highest contaminant vapor concentration in the subslab during the preferential pathway open period could have been order of magnitude higher than recorded. The complexity of the predicted α_{subslab} that concentrations profiles in Figure 1.16 suggest that use of any single collected concentration value to characterize the whole subslab is very dangerous.

This highlights the large impact that a preferential pathway can have on subsur-

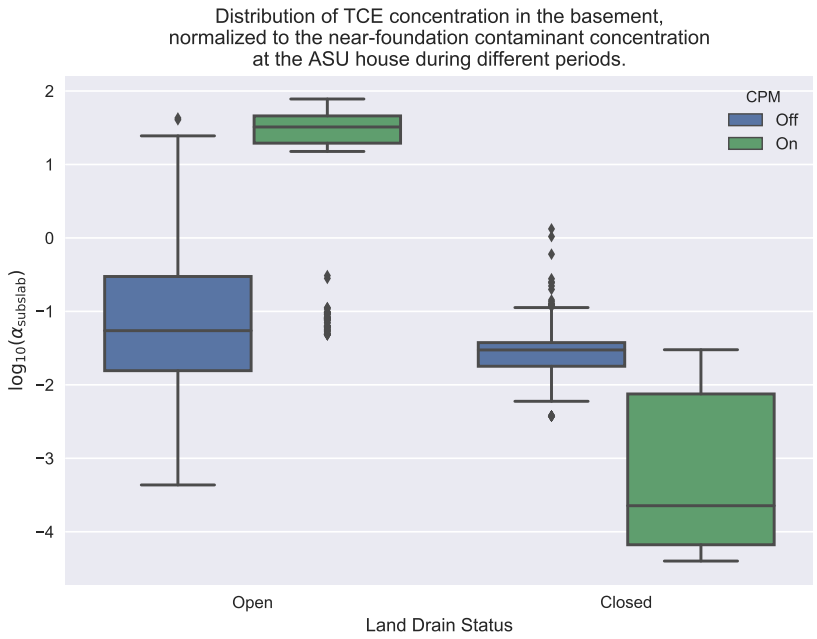

Figure 1.16: Boxplot showing the distribution of α_{subslab} considering the effects of CPM and the ASU house land drain preferential pathway. Here α_{subslab} is the attenuation from sub-slab sampling location 5 to the indoor environment. The box signifies the interquartile range (IQR) of values, with the central line representing the median value, and the top and bottom of the box are the 25th and 75th percentiles. The whiskers extend to 1.5 times the IQR. Markers indicate outlier data points that fall outside the whiskers.

face spatial contaminant concentrations. However, another possibility for explaining such high α_{subslab} values is that they may indicate that there are some indoor contaminant sources present. This was not however the situation at the ASU house. Therefore, this is another aspect of VI that investigators should be cognizant of very large α_{subslab} values could be an indicate an indoor source *or* the existence of some preferential pathway at the VI site.

1.5.2 EPA Duplex

The spatial variability of the soil-gas contaminant concentration at the EPA duplex is investigated by interpolating the recorded data using the kriging technique. Kriging is a commonly used technique in geostatistics where sparse spatial data can be interpolated over a larger spatial grid. This interpolation is performed by calculating the spatial covariance between the known data points, making assumptions of

spatial data distribution model - defining a kernel, and then fitting parameters to these kernels.

Soil-gas contaminant concentration data was collected at multiple locations and at multiple depths. In Figure 1.5b we can see a number of ports labeled as SSP and SGP - these are the locations where soil-gas concentration data were collected. Using the length scale in Figure 1.5b, approximate x and y coordinates for the location of each sampling port are extracted from the figure, and the bottom left corner of the figure is defined as $(x, y) = (0, 0)$. In the publicly available EPA duplex database[**noauthor˙indianapolis˙nodate**], the concentration of various contaminant at 5 different depths across time are recorded. These together form a large dataset where soil-gas contamination concentration, their spatial coordinates in three dimensions, across time, for various contaminants, are known.

Kriging generally performs best if the input data is normally distributed, which the soil-gas contamination data generally not, but after a $\log_{10}$ transformed it is generally normally distributed. The kriging is performed using the SciKit-learn Python package[**pedregosa˙scikit-learn˙2011**]. This requires input data, the data coordinates, a grid to which data is to be interpolated onto, and a kernel.

A radial-basis function kernel, multiplied by a constant is here chosen, as it closely resembles the solution to the infinite domain diffusion equation.

$$k(\vec{x}_i, \vec{x}_j) = C \exp\Big(-\frac{1}{2} d\Big(\frac{\vec{x}_i}{l}, \frac{\vec{x}_j}{l}\Big)\Big) \tag{1.4}$$

k is the kernel output value that determines the interpolated soil-gas concentration; $\vec{x}_i, \vec{x}_j$ are the coordinates for some points i and j; C is a constant that is determined by the software; $d\Big(\frac{\vec{x}_i}{l}, \frac{\vec{x}_j}{l}\Big)$ is the distance between $\vec{x}_i$ and $\vec{x}_j$, scaled by a length parameters l, which is determined by the software.

The results of the kriging is plotted using Plotly[**plotly˙technologies˙inc.˙collaborative˙nodate**] in Figure 1.17. It should be noted that these are soil-gas contaminant concentrations each from a period that is (by inspection) determined to be relatively "representative" of the overall temporally separated dataset; soil-gas contaminant concentra-

tions fluctuate spatially in time, but there are some general trends.

Figure 1.17 show how varied the soil-gas spatial variability for different contaminants can be. In particular, we see that trichloroethene (TCE) here exhibit relatively minor spatial variability compared to chloroform or tetrachloroethene (PCE). A likely explanation for this disparity is the role that the sewer played at this site.

In a later study of the EPA duplex, **mchugˑevidenceˑ2017**[**mchughˑevidenceˑ2017**] found that PCE and chloroform could be found throughout the sewer network in the neighborhood. Looking again at PCE and chloroform in Figure 1.17, we see that there is often a "hot spot" in the middle slice, approximately at a depth of $-2.75\,\mathrm{m}$, roughly in the middle of the front lawn area. This is roughly the spot where the sewer line connected to the EPA duplex was, which suggest that there is a leak in that vicinity. The leak in that particular area, and thus the sewer preferential pathway at the site, is likely what significantly contributes to much the soil-gas contaminant concentration spatial variability. This shows another way that a preferential pathways can the play a significant role at a VI site, and the importance of screening for them during a VI site investigation.

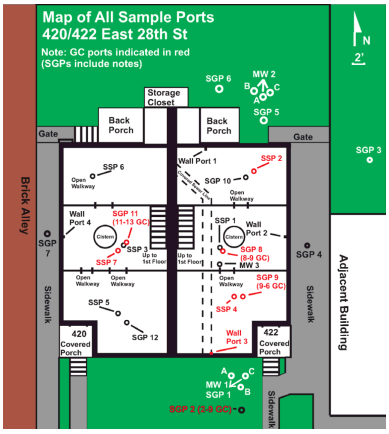

(a) Floorplan of the EPA duplex. The soil-gas figures x & y coordinates are relative to the bottom left corner.

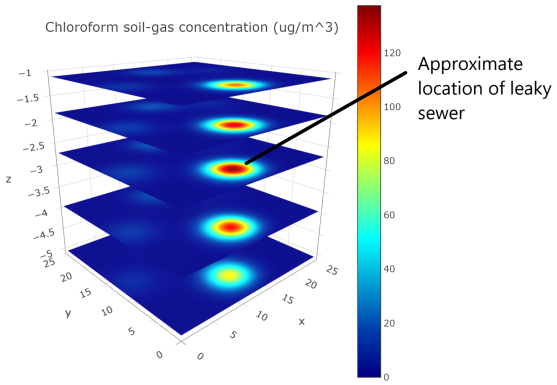

(b)

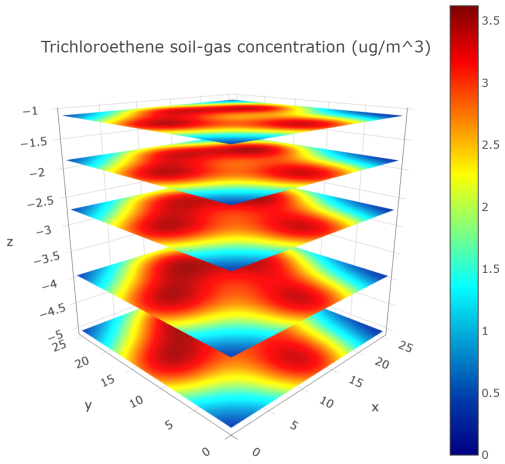

(c)

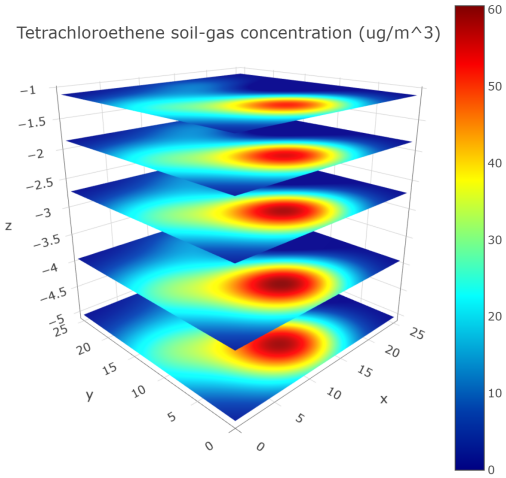

(d)

Figure 1.17: Interpolated soil-gas contaminant concentrations for select contaminant underneath the EPA duplex. Soil-gas concentrations profiles reveal a potential leak in the sewer line roughly underneath the EPA duplex front lawn.